Article

Theoretical Investigation of the "CO in"–"CO out" Isomerization in a [2Fe–2S] Ferredoxin: Free Energy Profiles and Redox States

Francesco Pizzitutti, Pierre Stif, and Massimo Marchi

J. Am. Chem. Soc., **2003**, 125 (49), 15224-15232• DOI: 10.1021/ja0370286 • Publication Date (Web): 12 November 2003

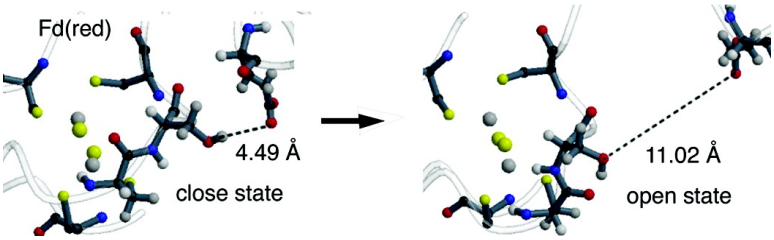

More About This Article

Additional resources and features associated with this article are available within the HTML version:

- Supporting Information
- Access to high resolution figures
- Links to articles and content related to this article
- Copyright permission to reproduce figures and/or text from this article

View the Full Text HTML

J|A|C|S
ARTICLES
Published on Web 11/12/2003

Theoretical Investigation of the "CO in"−"CO out" Isomerization in a [2Fe−2S] Ferredoxin: Free Energy Profiles and Redox States

Francesco Pizzitutti,[†,‡] Pierre Sétif,[§] and Massimo Marchi*[,†]

Contrinution from the Commissariat à l'Énergie Atomique, DSV-DBJC-SBFM, Centre d'Études, Saclay, 91191 Gif-sur-Yvette Cedex, France, Commissariat à l'Énergie Atomique, DSV-DBJC-SBE/CNRS URA 2096, Centre d'Études, Saclay, 91191 Gif-sur-Yvette Cedex, France, and Dipartimento di Fisica, Università degli Studi di Roma "La Sapienza", p.le A. Moro 2, 00185 Roma, Italy

Received July 2, 2003; E-mail: mmarchi@cea.fr

Abstract: This paper reports on extensive molecular dynamics simulations (about 40 ns in total) in both the reduced and the oxidized states of Ferredoxin from Cyanobacterium *Anabaena* PCC7119. These calculations have provided us with the free energy profile of the ϕ_{47} backbone angle which controls the "CO in" to "CO out" transition of Cys46 in the reduced and oxidized Fd7119. Our main motivation has been to identify the time scales involved in the reduction of Fd and single out the amino acid residues crucially affecting the conformational change and, thus, electron transfer. The free energy profiles obtained in this study are relevant to electron transfers in the PSI/Fd7119 and Fd7119/FNR complexes. Our findings based on hydrated ferredoxin simulations are that activated processes are to occur in the protein during electron transfer to and from ferredoxin. The relative stability and the activation barrier of the "CO in" to "CO out" transition can be modulated by the distance between the Ser47 and the Glu94 residues. In our calculations, for short distances, the "CO in" state is favored in the reduced form, whereas for large distances, the "CO out" state becomes increasingly favored. Accordingly, conformational changes in Fd7119 when bound to PSI or FNR can have crucial effects on the kinetics of the electron transfer. Our simulations also show that the hydrogen bond between between Ser47(OG) and Cys46(O) is essential to lock in the "CO out" state. This finding explains why only the Ser47Thr Fd7119 mutant sustains electron transfer activity, as only residues serine and threonine can form a specific hydrogen bond with Cys46(O). Finally, our simulations predict that Phe65 has a large probability of being in close contact with the Cys46(O) at the top of the conformational free energy barrier. This carbonyl/phenyl ring interaction can then facilitate the de-localization of the Fd's electron toward the Π orbitals of Phe65 aromatic ring which is thought to be crucial to the Fd7119/FNR electron transfer

I. Introduction

Ferredoxins (Fd) are small (10−11 kDa), globular, strongly acidic proteins, found in bacteria plants and mammals. In plants, algae, or photosynthetic cyanobacteria, Fd's are the direct recipients of the electron pathway from photosystem I (PSI). These "plant type" Fd's are a source of low-potential electrons for many reductive processes such as the NADPH synthesis catalyzed by the ferredoxin-$NADP^+$ reductase (FNR). The "plant type" Fd contains a [2Fe−2S] cluster, where two sulfur atoms bind two irons, tetrahedrally coordinated by four cysteine sulfur atoms.[1,2] In the oxidized and reduced Fd's, the [2Fe−2S] cluster is charged +2 and +1 *e*, which corresponds to iron valence states of ($Fe^{3+}Fe^{3+}$) and ($Fe^{3+}Fe^{2+}$), respectively.[3]

In the last years, several biochemical, kinetic, and structural studies have been performed to elucidate the electron transfer (ET) mechanism from PSI to Fd and from Fd to FNR.[4,5] Combined mutagenesis and kinetic studies have shown that three residues, Ser47, Phe65, and Glu94, have a crucial importance in determining the rate constant in the ET process between ferredoxin from cyanobacterium *Anabaena* and FNR. Mutated Fd's in these positions experience a reduction of the ET rate constant of more than 4 orders of magnitude without drastically altering the redox potential of the complex. The mechanism of ET implying Fd's is also complicated by molecular recognition which occurs before and after the ET event. Indeed, for the transfer between PSI and ferredoxin from *Synechocystis* sp. PCC6803, three different time scales were detected by laser flash absorption spectroscopy studies[6] and associated to protein

[†] Commissariat à l'Énergie Atomique, DSV-DBJC-SBFM, Centre d'Études.
[‡] Dipartimento di Fisica, Università degli Studi di Roma "La Sapienza".
[§] Commissariat à l'Énergie Atomique, DSV-DBJC-SBE/CNRS URA 2096, Centre d'Études.

(1) Holm, R.; Kennepohl, P.; Solomon, E. *Chem. Rev.* **1996**, *96*, 2239.
(2) Johnson, M. *Cur. Opin. Chem. Biol.* **1998**, *2*, 173.
(3) Beinert, H.; Holm, R.; Münck *Science* **1997**, *277*, 653.
(4) Setif, P. *Biophys. Acta* **2001**, *1507*, 161.
(5) Hurley, J. K.; Morales, R.; Martinez-Julvez, M.; Brodie, T. B.; Medina, M.; Gomez-Moreno, C.; Tollin, G. *Biochim. Biophys. Acta* **2002**, *1554*, 5.
(6) Setif, P.; Bottin, H. *Biochemistry* **1994**, *33*, 8495.

10.1021/ja0370286 CCC: $25.00

configurational transitions, complex formations and/or solvation shell rearrangement.

Although X-ray structures of various "plant type" Fd's[7,8] and FNR−Fd complexes[9,10] have been available for a certain time, the docking of Fd to PSI is still a challenging topic.[11] More recently, X-ray structures of Fd from *Anabaena* PCC7119 (Fd7119) were resolved both for the oxidized (**oxi**) and reduced (**red**) forms.[12] The comparison between the two structures showed an important redox-linked conformational change: In the oxidized structure, the carbonyl oxygen of the Cys46 backbone, is oriented toward the [2Fe−2S] cluster ("CO in" configuration). In the reduced crystal instead, Fd7119 shows an alternative conformation in which the same carbonyl oxygen points away from the cluster ("CO out" configuration). Thus, the "CO in"−"CO out" isomerization in Fd is directly coupled to the reduction of the [2Fe−2S] cluster, when Fd binds to PSI, and also to its subsequent oxidation when the Fd/FNR complex is formed.

So far theoretical investigations of electron transfer in Fd's have focused on the electronic structure of the [2Fe−2S] cluster and the coupling with neighboring residues. In a first paper, J. Li et al.[13] applied a combined density functional theory (DFT) and dielectric continuum model to the active site Fd from *Anabaena* 7120 in order to compute the charge distribution around the [2Fe−2S] cluster and to estimate its redox potential. In a subsequent paper, R. Morales et al.[14] studied the active site at a higher level of theory including explicitly the amino acids of the [2Fe−2S] cluster first solvation shell. Their investigation suggested a specific role for Glu94 and the Ser47 carbonyl in the regulation of the electron charge delocalization from the atom Ser47(OG) to the aromatic ring of Phe65. Accordingly, the negatively charged Glu94 favors an increase in electron density on the aromatic ring of Phe65. As argued by site-directed mutagenesis and supported by structural studies,[15] the residue at position 65, strategically bridging the two cofactors of the Fd/FNR complex, is crucially important for the rapid ET in *Anabaena* Fd.

In this investigation, we have used molecular dynamics (MD) methods to study the "CO in"−"CO out" isomerization in hydrated Fd7119. To this purpose, extensive simulations have been carried out (about 40 ns in total) to compute the free energy surface to go from the "CO in" to the "CO out" state in both the reduced and oxidized states. Our main motivation has been to identify the time scales involved in the reduction of Fd and single out the amino acid residues crucially affecting the conformational change and, thus, electron transfer.

This paper is organized as follows: Section II discusses the molecular dynamics methods and techniques used to compute the free energy profile of the "CO in"−"CO out" isomerization in hydrated Fd7119. Section III presents: First, the simulations structural results for the hydrated protein; second, the computed free energy profiles in solution and in the crystal environments. The paper ends with a section devoted to the chemical and biochemical conclusions that can be derived from our study.

II. Methods

A. Molecular Dynamics Simulation. The free energy results discussed in this paper were obtained from MD simulations of Fd7119 in water solutions and in the crystal environment. All simulations were performed with parallel and scalar versions of the program ORAC.[16,17] The code implements highly efficient MD techniques for sampling of biomolecular systems based on a multiple time scale approach. The simulations in the NPT ensemble allowed only for isotropic cell volume fluctuations and used a technique, described in ref 18, combining an r-RESPA (reversible REference System Propagation Algorithm)[19] algorithm with smooth particle mesh Ewald.[20] For the latter, a convergence parameter $\alpha = 0.43$ Å^{-1}, a 64-point grid in each direction and an interpolating 5*th* order B-spline parameter were used. The barostat and thermostat parameters were those used in ref 18. Bond stretching involving hydrogen atoms were frozen by standard constraint techniques.[21−23]

Whereas the protein was modeled by CHARMM27—an improvement on the all-atom force field described in ref 24—the TIP3P model[25] was used to describe water. For cross interactions, the standard mixing rules were used for the van der Waals parameters. For all ionizable residues of the simulated protein, we chose their most stable ionic forms in solution at pH 7 to model their atomic charges.

The charge distribution on and in the vicinity of the [2Fe−2S] cluster was taken from ref 13. There, the ESP (ElectroStatic Potential fit) charges of the **oxi** end **red** states were derived by performing a DFT calculation on the Fd7119 [2Fe−2S] cluster and the four cysteines covalently bound to the two irons. Bond lengths and angle bendings within the [2Fe−2S] cluster and between the cluster and its 4 ligands were added by us to account for structural data (see Figure 1 and Table 1).

In all of the solution MD runs, the periodically replicated simulation box was a truncated octahedron with side length of 65.47 Å. This choice corresponds to a primitive bcc cell of axes $a = b = c = 56.7$ Å and angles $\alpha = \beta = \gamma = 109.47°$. Simulations of Fd7119 in solution were performed for two different solvation environments: A first one (simulations labeled *no ions*) in which only water molecules were added; and a second one including water and ions (labeled *ions*) specifically $5Cl^-$ and $24Na^+$ corresponding to an ionic strength of 0.18 M. In both *no ions* and *ions* simulations, water molecules were added around the protein X-ray structures until the density of water at the desired pressure and temperature of systems was attained. In the *ions* simulations, ions

(7) Holden, H.; B. L., J.; J. K., H.; Tollin, G.; Oh, B.; Skjeldahl, L.; Chae, Y.; Cheng, H.; Xia, B.; J. L., M. *J. Bioenerg. Biomembr* **1994**, *26*, 67.
(8) Hurley, J. K.; abd Morales, R.; Martinez-Julvez, M.; Brodie, T.; Medina, M.; Gomez-Moreno, C.; Tollin, G. *BBA-Bioenergetics* **2002**, *1554*, 5.
(9) Morales, R.; Kachalova, G.; Vellieux, F.; Charon, M.; Frey, M. *Acta Crystallogr. D* **2000**, *56*, 1408.
(10) Kurisui, G.; Kusunoki, M.; Katoh, E.; Yamazaki, T.; Teshima, K.; Onda, Y.; Kimata-Ariga, Y.; Hase, T. *Nat. Struct. Biol.* **2001**, *8*, 117.
(11) Setif, P.; Fischer, N.; Lagoutte, B.; Bottin, H.; Rochaix, J.-D. *Biochim. Biophys. Acta* **2002**, *1555*, 204.
(12) Morales, R.; Chron, M.; Hudry-Clergeon, G.; Pétillot, Y.; Norager, S.; Medina, M.; Frey, M. *Biochemistry* **1999**, *38*, 15 764.
(13) Li, J.; Nelson, M. R.; Peng, C. Y.; Bashford, D.; Noodleman, L. *J. Phys. Chem. A* **1998**, *102*, 6311.
(14) Morales, R.; Frey, M.; Mouesca, J. *J. Am. Chem. Soc.* **2002**, *124*, 6714.
(15) Hurley, J.; Cheng, H.; Xia, B.; Markley, J.; Medina, M.; Gomez-Moreno, C.; Tollin, G. *J. Am. Chem. Soc.* **1993**, *115*, 11 698.
(16) Procacci, P.; Darden, T.; Pacy, E.; Marchi, M. *J. Comput. Chem.* **1997**, *18*, 157.
(17) Procacci, P.; Marchi, M. In *Advances in the Computer Simulations of Liquid Crystals*; Zannoni, C., Pasini, P., Eds.; Proceedings of the NATO-ASI School, Erice 11−21 June 1998, Dodrecht The Netherlands 1999; Kluwer Academic: 1999; 333.
(18) Marchi, M.; Procacci, P. *J. Chem. Phys.* **1998**, *109*, 5194.
(19) Tuckerman, M.; Berne, B. J.; Martyna, G. J. *J. Chem. Phys.* **1992**, *97*, 1990.
(20) Essmann, U.; Perera, L.; Berkowitz, M. L.; Darden, T.; Lee, H.; Pedersen, L. G. *J. Chem. Phys.* **1995**, *103*, 8577.
(21) Ryckaert, J.-P.; Ciccotti, G.; Berendsen, H. *J. Comput. Phys.* **1977**, *23*, 327.
(22) Andersen, H. C. *J. Comput. Phys.* **1983**, *52*, 24.
(23) Ciccotti, G.; Ryckaert, J.-P. *Computer Phys. Rep.* **1986**, *4*, 345.
(24) MacKerell, A., Jr.; Bashford, D.; Bellot, M.; Dunbrack, R., Jr.; Evanseck, J.; Field, M.; Fischer, S.; Gao, J.; Guo, H.; Ha, S.; Joseph-McCarthy, D.; Kuchnir, L.; Kuczera, K.; Lau, F.; Mattos, C.; Michnick, S.; Ngo, T.; Nguyen, D.; Prodhom, B.; W. R., II.; Roux, B.; Schlenkrich, M.; Smit, J. Q.; Stote, R.; Straub, J.; Watanabe, M.; Wiorkiewicz-kuczera, J.; Yin, D.; Karplux, M. *J. Phys. Chem B* **1998**, *102*, 3586.
(25) Jorgensen, W. L.; Chandrasekhar, J.; Madura, J. D.; Impey, R. W.; Klein, M. L. *J. Chem. Phys.* **1983**, *79*, 926.

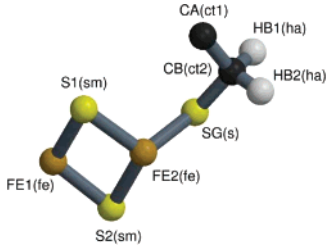

Figure 1. Protein Data Bank atomic labels of the [2Fe−2S] cluster and of the residue Cys46. In bracket are reported the corresponding CHARMM27 labels.

Table 1. Intramolecular Parameters for the [2Fe−2S] Cluster and Its Neighboring Atoms[a]

bond		
atoms	K_r	r_0
s fe	250.0	2.225
bendings		
atoms	K_θ	θ_0
s fe s	50.00	104.06
fe s fe	50.00	75.94
fe sm ct2	20.00	110.00
sm sm fe	72.50	103.30
sm fe s	25.00	112.07
sm fe sm	75.00	106.23
sm sm ct3	72.50	103.30
sm sm ct2	72.00	103.30
ss cs ct3	55.00	118.00
ss cs ha	40.00	112.30
torsion proper		
atoms	V_ϕ	n γ
fe s fe s	3.5000	2 180.0

[a] The functional form of the CHARMM27 potential has been retained for these additional interactions. Distances are in Å, energies in kcal mol^{-1} and angles in degree.

were added by substituting a water molecule around a protein charged group with ions of opposite charge until the imposed ionic strength was obtained. In all systems discussed here, ferredoxin was hydrated on averaged by about 4090 water molecules.

Two different protocols have been applied to set up and equilibrate the simulated systems. In the protocol named **hard start**, or *hs*, the protein, without its crystallographic water molecules, was initially minimized by conjugated gradient for 100 steps to remove close van der Waals contacts, and then hydrated. The system was subsequently heated by increasing monotonically the temperature, T, from 0 to 300 K in 120 ps. Specifically, each 0.012 ps the atomic velocities were rescaled to attain a temperature $T = T + \Delta T$, where ΔT was chosen so that $T = 300$ K after 120 ps. Two additional equilibration runs were then performed: 120 ps at constant volume and $T = 300$ K, and then 120 ps at $P = 0.1$ MPa and $T = 300$ K.

The second protocol called **soft start**, or *ss*, assured a better equilibration of the solvent environment. This protocol was identical to *hs* except that after the initial minimization of the Fd7119 protein and subsequent hydration, two simulations of 120 ps were carried out with harmonic constraints on the Fd7119 atoms at $T = 400$ K and then $T = 300$ K. The restraining harmonic potential had a force constant $K_r = 400$ kcal mol^{-1} Å^2. The *ss* simulations then proceeded by heating the system to 300 K and with two additional runs in the NVT and NPT ensembles as for the *hs* protocol.

Whereas the *no ions* simulations were equilibrated by both *hs* and *ss* protocols, only the latter was used for *ions* simulations to obtain fast ions equilibration in the electrostatic field of a very acidic protein (e.g., total charge of **red** Fd7119 at pH 7 is of -19 *e*).

Two different initial structures were used in simulations of reduced and oxidized forms of Fd7119. The latter were started from the X-ray structure from reference[12] [Protein Data Bank (pdb) entry code 1QT9]. The simulations of the reduced forms used instead the crystallographic molecule A, alternate location B,[40] of the X-ray structures[12] [pdb entry code 1CZP].

After the initial equilibration runs, *hs* or *ss*, the systems of hydrated Fd7119's were placed at constant V and at $T = 300$ K and run further. We carried out (i) a 10 ns run of the reduced protein, no ions, soft start (FdR^{ni}_{ss}); (ii) a 10ns run of the reduced form, ions, soft start (FdR^{i}_{ss}); (iii) a 980 ps run of the reduced form, no ions, hard start (FdR^{ni}_{hs}); (iv) a 2 ns run of the oxidized form, no ions, soft start (FdO^{ni}_{ss}); (v) a 1 ns run of the oxidized form, ions, soft start (FdO^{i}_{ss}); and (vi) a 1 ns run of the oxidized form, no ions, hard start (FdO^{ni}_{hs}).

An additional *ss*, no ions, run of 300 ps has also been performed for the reduced Fd7119 in crystal environment. The orthorhombic forms of reduced Fd7119 have been obtained from ref 12 [pdb entry code 1CPZ]. The asymmetric unit of the orthorhombic **red** Fd7119 crystal contains 2 Fd7119 monomers. The simulation box was constructed by applying the 4 P $2_12_12_1$ symmetry operations to the asymmetric units producing 8 independent Fd7119 monomers. The subsequent solvation and set up operations were identical to those for *ss*, *no ions* solution simulations.

B. Umbrella Sampling and WHAM Approach. The umbrella sampling technique, introduced by Torrie and Valleau,[26] is widely employed in simulations of biomolecules to compute free energy profiles along conformational variables. It consists of adding a restraining potential, a function of a given conformational variable ξ, to the unperturbed Hamiltonian. Usually, n short simulations are carried out using n different potentials, $V_i(\xi)$, $i = 1, ..., n$, restricting the sampling of the coordinate ξ to n well-defined regions of the conformational space. The resulting n probability distributions $P_{oi}(\xi)$, corrected of the bias potential, can be related to the unbiased probability in the original ensemble spanned by the unperturbed Hamiltonian. The weighted histogram (WHAM) technique provides the best estimate of the potential of mean force profiles from a set of biased simulations.[27] In this approach, the n calculated probability distributions $P_{oi}(\xi)$ are superimposed in a weighted sum as

$$P_o(\xi) = \sum_{i=1}^{n} \omega_i(\xi) e^{\beta V_i} \frac{Z_o}{Z_{oi}} P_{oi}(\xi) \qquad (1)$$

Subjected to the condition

$$\sum_{i=1}^{n} \omega_i(\xi) = 1 \qquad (2)$$

where Z_o and Z_{oi} are the partition functions of the biased and unbiased ensembles, respectively. The weighting factors $\omega_i(\xi)$ are derived by

(26) Torrie, G. M.; Valleau, J. P. *Chem. Phys. Lett.* **1974**, *28*, 578.
(27) Ferrenberg, A. M.; Swendsen, R. H. *Phys. Rev. Lett.* **1989**, *63*, 1195.
(28) Sterpone, F.; Ceccarelli, M.; Marchi, M. *J. Mol. Biol.* **2001**, *311*, 409.
(29) Marchi, M.; Sterpone, F.; Ceccarelli, M. *J. Am. Chem. Soc.* **2002**, *124*, 6787.
(30) Marchi, M. *J. Phys. Chem. B* **2003**, *107*, 6598.
(31) Ibragimova, G.; Wade, R. *Biophys. J.* **1998**, *74*, 2906.
(32) Rypniewski, I.; Breiter, D.; Bennins, M.; Wesemberg, G.; Ho, B.; Markley, J.; Rayement, I.; Holde, H. *Biochemistry* **1991**, *30*, 4126.
(33) Shelley, J. C.; Sprik, M.; Klein, M. L. *Langmuir* **1993**, *9*, 916.
(34) Marchi, M.; Akasaka, K. *J. Phys. Chem. B* **2001**, *105*, 711.
(35) Cornell, W. D.; Cieplak, P.; Bavly, C. I.; Gould, I. R.; Merz, K. M., Jr.; Ferguson, D. M.; Spellmeyer, D. C.; Fox, T.; Caldwell, J. W.; Kollmann, P. *J. Am. Chem. Soc.* **1995**, *117*, 5179.
(36) Ceccarelli, M.; Marchi, M. *J. Phys. Chem. B* **2003**, *107*, 5630.
(37) Sterpone, F.; Ceccarelli, M.; Marchi, M. *J. Phys. Chem. B* **2003**, *107*, 11 208.
(38) Hurley, J.; Weber-Main, A.; Stankovich, M.; Benning, M.; Thoden, J.; Vanhooke, J.; Holden, H.; Chae, Y.; Xia, B.; Cheng, H.; Markley, J.; Martinez-Julvez, M.; GomezMoreno, C.; Schmeits, J.; Tollin, G. *Biochemistry* **1997**, *36*, 11 100.
(39) Brettel, K. *Biochim. Biophys. Acta* **1997**, *1318*, 322.
(40) Two Fd7119 conformations are found for each of the two crystallographic molecules: Alternate location A, and alternate location B.

imposing the minimization of the statistical error $\delta^2 P_o(\xi) = \langle P_o(\xi)^2 \rangle - \langle P_o(\xi) \rangle^2$ in the estimate of the unbiased probability distribution. The resulting expression for $P_o(\xi)$ are the WHAM equations

$$P_o(\xi) = \frac{\sum_{i=1}^{n} n_i P_{oi}(\xi) e^{\beta V_i(\xi)}}{\sum_{j=1}^{n} n_j e^{f_j - \beta V_j(\xi)}} \quad (3)$$

and

$$e^{-f_j} = \int d\xi P_{oj}(\xi) \quad (4)$$

Here, n_i ($i = 1, ..., n$) is the number of snapshots from the i-th simulation, n is the number of simulations, the restraining potential of the i-th simulation is $V_i(\xi)$, and $f_j = \beta_j a_j$ is the free energy of the system biased by the potential $V_j(\xi)$. The WHAM equations are then solved self-consistently, starting from arbitrarily chosen values for the f_j and solving iteratively until convergence.

The WHAM technique has been used in our study to compute the free energy profiles of the "CO in" to "CO out" transition. This isomerization involves a simple rotation around the ϕ backbone torsion angle of the Fd's residue Ser47, or ϕ_{47}, defined by the four atoms: C(*Cys*46), N(*Ser*47), C_α(*Ser*47), C(*Ser*47).

Thus, the "CO in" to "CO out" transition was obtained by imposing a set of restraining potential $V_i(\phi)$ of the form

$$V_i(\phi) = K_i(\phi - \phi_i)^2 \quad (5)$$

With ϕ the angle ϕ_{47} and K_i the force constant.

Initially, we chose 12 ϕ_i distributed uniformly from 0 to 360°, and a value of K_i equal to 10 kcal mol^{-1}. Three additional runs were then performed in regions not sufficiently sampled by the first 12 runs. In these runs, the constants K_i were chosen greater than 10 kcal mol^{-1} in a range from 10 to 20 kcal mol^{-1}. For $i = 1$ the starting structure was always the last configuration of the long equilibration runs. For $i > 1$ the initial structures were the final configurations of the $(i - 1)$-th runs. In each window, the system was equilibrated for 5 ps and then run for additional 95 ps of production. In total, the time for all windows of each simulated system was 1425 ps. Values of the angle ϕ_{47} were recorded every 2 fs. Then, the WHAM equations were iteratively solved until the absolute change of the f_i in eq 4, in each window, was less than 0.05 kcal mol^{-1}.

III. Results

A. Structure and Interactions of Fd7119 in Solution. The simulated system showed a different degree of stability depending not only on the setup protocol, as anticipated by the previous section, but also on the solvation environment and on the Fd7119 redox state. The time history of the root-means square deviation (RMSD) from the X-ray structure are reported in Figure 2 for all our trajectories. RMSD is computed after performing a rigid body fit—only rigid rotations and translations are allowed—of the two structures to minimize the deviation.

The effect of the preparation protocol is clearly seen in Figure 2b where trajectory FdR^{ni}_{hs} is compared with the first ns of FdR^{ni}_{ss}. Here, the RMSD for FdR^{ni}_{hs} arrives at ~3.2 Å, whereas FdR^{ni}_{ss} is stable at around 1.2 Å. In general, for the trajectories that started with the *ss* setup protocol, a much more stable behavior is obtained. This is also true for simulations in the oxidized state, see Figure 2c, although the *hs* simulation reaches a RMSD smaller than that of the *hs* simulation of the reduced state.

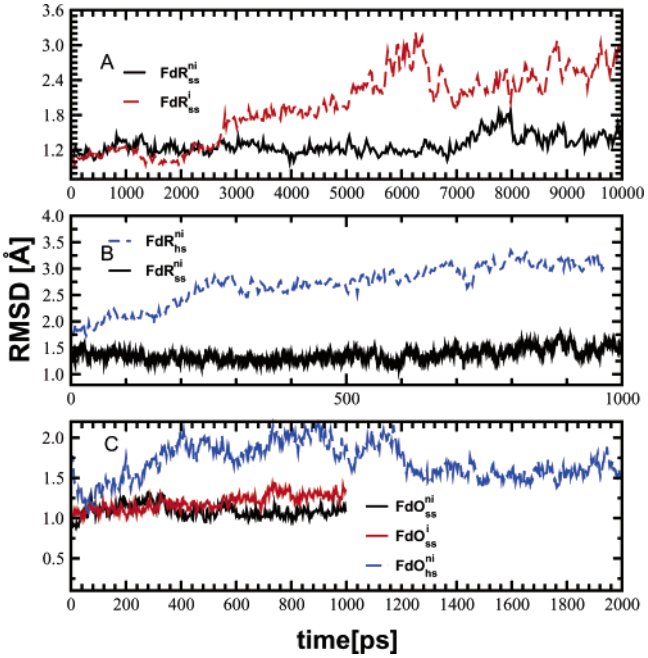

Figure 2. Root-mean-square deviations (RMSD) of the simulated Fd proteins from the X-ray structure: FdR^{ni}_{ss} and FdR^{i}_{ss} are in panel **a**; FdR^{ni}_{hs} and the first 1000 ps of FdR^{ni}_{ss} are in panel **b**; while panel **c** displays simulations FdO^{ni}_{ss}, FdO^{i}_{ss} and FdO^{ni}_{hs}. Only the C_α carbons are included in the RMSD calculations. To reduce the noise, data presented in panel **a**, **b**, and **c** have been averaged out over 24, 2.4, and 2.4 ps, respectively.

The stabilization of the structure obtained with the *ss* protocol is related to the exceptionally high density of negatively charged residues on the protein surface (−19 *e* total net charge in the reduced state). Indeed, negatively charged residues strongly repel each other when not sufficiently screened by the solvent molecules. This interaction can destabilize the overall protein structure, thus leading to an increase in the RMSD. With the *ss* setup protocol instead, the solvent molecules are preequilibrated in the electrostatic field generated by the harmonically restrained Fd7119 protein. In the past, protocols similar to *hs* used here produced structurally stable proteins in multi-nanosecond simulations of soluble globular proteins such as BPTI, lysozyme, and T4-lysozyme, which have a much lower charge density than Fd7119.[28−30]

The simulation FdR^{i}_{ss} also shows a steady increase of RMSD to ~3.0 Å after 10 ns, whereas RMSD of FdR^{ni}_{ss} remains close to 1.2 Å all along the trajectory. In contrast, shorter MD simulations—less than a ns—of small size proteins of marginal stability had smaller RMSD when carried out in ionic solutions rather than in water alone.[31]

As shown in Figure 2c, whereas the RMSDs of the FdO^{ni}_{ss} and FdO^{i}_{ss} simulations reach a stable plateau at around 1 Å, simulation FdO^{ni}_{hs} has a larger deviation from X-ray. For the latter, RMSD reaches 1.7 Å after 2 ns which is smaller than that of simulation FdR^{ni}_{hs} in the reduced state.

We have also computed the average backbone coordinates for the six trajectories. A pictorial view of these average conformations obtained for the reduced and oxidized states of Fd7119 are shown in Figure 3 , panel a and b, respectively. For all reduced and oxidized structures the largest deviations from the X-ray backbone (in green in the pictures) are in the C-terminus, whereas for FdR^{ni}_{hs} differences are also noticeable in the region near Ala11 and Phe65.

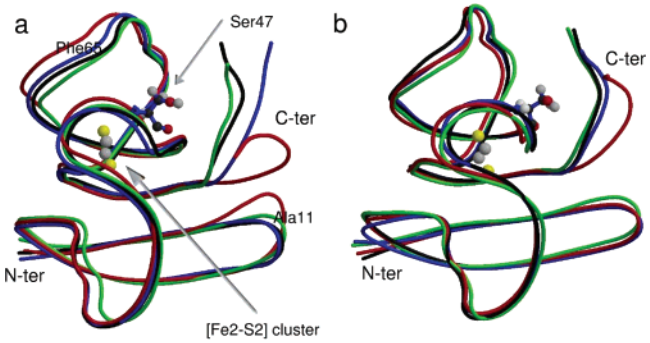

Figure 3. Comparison of the average backbone conformation obtained from the MD trajectories of hydrated Fd. In panel **a**, we compare the average conformations for the **red** Fd7119 runs FdR^{ni}_{ss} (in black), Fd (in blue), FdR^{ni}_{hs} (in red) with X-ray (green). Panel **b** shows results for **oxi** Fd7119 runs FdO^{ni}_{ss} (black), FdO^{i}_{ss} (blue), FdO^{ni}_{hs} (red) and X-rays (green). For reference to the reader [2Fe−2S] cluster and Ser47 are shown in ball-and-sticks.

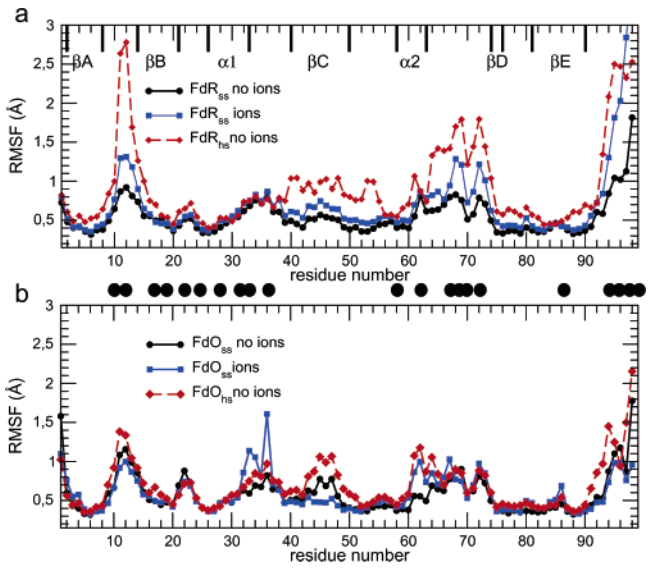

Figure 4. Average root-mean-square fluctuations (ARMSF) as a function of the residue number obtained from the three reduced (panel **a**) and the three oxidized (panel **b**) Fd7119 trajectories. ARMSF are always averaged over 1ns time intervals. Only the ARMSF of C_α are plotted. Negatively charged residues Asp and Glu are marked by a black circle between the panels. On the top of panel **a** we display the secondary structure of the Fd7119 protein following the nomenclature of ref 32.

Information on the flexibility and stability of the protein backbone can be derived from the analysis of average root-means square fluctuations, or ARMSF, of the C_α's. The ARMSF averaged over 1 ns is shown in Figure 4 for the six simulations. For the simulations longer than 1 ns, the ARMSF's were averaged over the maximum number of consecutive 1 ns intervals in which the trajectory could be separated.

By visually inspecting panels a and b of Figure 4, we notice that the most stable reduced Fd7119 trajectories, FdR^{ni}_{ss} and FdR^{i}_{ss}, have backbone fluctuations very close in pattern to those of all the oxidized Fd7119 trajectories. On the contrary, ARMSF are larger for FdR^{ni}_{hs} especially in the four regions defined by residues 10−14, 39−56, 63−75, and the last five amino acids of the C-terminus. All these regions have a high density of negatively charged residues at pH = 7 as indicated by the black circles in Figure 4. The 39−56 region not marked in Figure 4 contains cofactor and its coordinated cysteines which are negatively charged.

Table 2. Distances between the Atoms of Glu94($OE^{1,2}$)'s and Ser47(OG) in the Crystallographic[12] and Simulated Fd7119 Structures[a]

X-ray red	*d* [Å]
mol. A	2.49
mol. B	2.92
X-ray oxi	***d*** **[Å]**
	2.50
Fd7119 solution runs	***d*** **[Å]**
FdR^{ni}_{ss}	9.06
FdR^{i}_{ss}	13.17
FdR^{ni}_{hs}	19.65
FdO^{ni}_{ss}	5.67
FdO^{i}_{ss}	8.43
FdO^{ni}_{hs}	17.77
Fd7119 solution runs	***d*** **[Å]**
mol. A	11.02
mol. B	4.49
mol. C	5.72
mol. D	5.59
mol. E	7.05
mol. F	6.49
mol. G	9.14
mol. H	3.86

[a] The symbol $OE^{1,2}$ indicates that of the atoms OE1 and OE2 we chose the closest to Ser47(OG).

Despite having been prepared with the same protocol as FdR^{ni}_{hs}, simulation FdO^{ni}_{hs} presents a backbone mobility similar to the results obtained from the other two simulations of oxidized Fd. Simulations FdR^{ni}_{hs} and FdO^{ni}_{hs} differ only for the charge of the cofactor [2Fe−2S] and for the two initial X-ray structures. We have also carried out a simulation in the reduced state and with the *hs* protocol, but using as initial conformation the oxidized Fd. The RMSD behavior resulting from this simulation was similar to that of FdO^{ni}_{hs} reaching 1.7 Å after 2 ns (data not shown). Hence, it is likely that the major effect on the large RMSD of FdR^{ni}_{hs} is due to strong and unscreened electrostatic interactions in the X-ray reduced structure. These interactions need to be damped by the solvent for the structure to be stable in our MD runs.

Some noticeable differences between the experimental and simulated Fd7119 structures are also found in the detail of the atomic interactions, in particular the hydrogen bonds (H-bonds). In the case of Fd7119, we notice that the H-bond linking Ser47-(OG) and Glu94(OE2), observed in experimental Ferredoxin from *Anabaena* X-ray structures,[7,12,32] is not conserved in our simulations (see Table 2). Indeed, for the oxidized and reduced Fd7119 the unfavorable electrostatic interactions between C-terminal−highly negatively charged−and the [2Fe−2S] cluster produces a conformational transition from a "close", to an "open", solvated, configuration. The latter is the most stable in our simulations because of the electrostatic screening of the water and ionic solutions.

This result might well be biased by the use of a fixed charge electrostatic model which enhances the importance of interactions between charged structures.[33] We have also shown in a previous study[34] that the CHARMM and AMBER[35] force fields are not capable of reproducing the geometric details of the intra-protein H-bonds. In the specific case of Fd7119, we observe, however, that H-bonds linking Glu94 and Ser47 (d_{OG-OE}) or their equivalent residues in other Fd7119's is not maintained

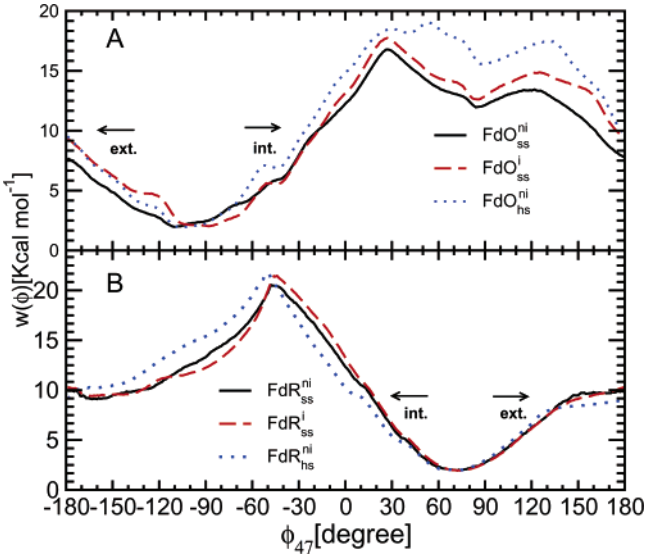

Figure 5. Free energy profiles for the torsion angle ϕ_{47} of **oxi** Fd, panel **a**, and of **red** Fd7119 panel **b**. The labels of the legends are explained in the text. The *internal* and *external* pathways for the "CO in"–"CO out" transition are labeled by two arrows and marked **int.** and **ext.**, respectively.

in X-ray structure of the complex between *Anabaena*, Ferredoxin, and FNR ($d_{OG-OE} = 3.97$ Å) and in the NMR structures of ferredoxin from parsley ($d_{OG-OE} = 4.01$ Å). We will show in the next sections that the mobility of this C-terminus is directly coupled to the reduction of Fd7119.

B. Free Energy Profiles for the "CO in"–"CO out" Transition. 1. Ferredoxin in Solution. The application of umbrella sampling and of the WHAM technique to the "CO in" to "CO out" transition in hydrated Fd7119 produced the free energy profiles presented in Figure 5. As discussed previously, the reaction coordinate for this conformational change is the backbone torsional angle ϕ_{47}. This free energy calculation was carried out for all of the 6 systems of hydrated Fd7119 discussed so far. We first noticed that all simulations in the oxidized and reduced state of the [2Fe−2S] cluster have well-defined minima. Very little difference is observed among curves with the same charge state which are not affected neither by ionic strength nor by the way the system was prepared and equilibrated. Not surprisingly, the major deviations are obtained for systems obtained with the *hs* protocol, as they have the largest RMSD deviation from the crystallographic structure.

For simulations of the reduced state (Figure 5b), very little difference is observed among the three curves. In all cases, a pronounced maximum at $\phi_{47} \approx -50°$ and a deep minimum at $\phi_{47} \approx 70°$ are found. These minima correspond to the "CO out" configuration, where the Cys46 carbonyl oxygen points away from the [2Fe−2S] cluster. No additional relative minima are found near the "CO in" conformation corresponding to a ϕ_{47} around −100°, as seen in the profiles of the oxidized Fd's. Instead, profiles FdR$^{ni}_{ss}$ and FdR$^{i}_{ss}$ experience a very shallow minimum near $\phi_{47} \simeq -160°$—less than 1 k_BT of activation barrier to relax to conformation "CO out".

As we will see more in detail in the next section, the interaction between the carbonyl of Cys46 and the OG−HG group of Ser47 is crucial for the stability of the "CO out" conformation. For ϕ_{47} close to the minimum of the free energy profiles and for all three simulations, we obtain the smallest distance between the two groups with $d_{O-OG} \simeq 2.70$ Å. Also, in FdR$^{ni}_{ss}$, the average angles between the atoms Cys46(C) Cys46(O)···Ser47(HG) and Cys46(C)Cys46(O)···Ser47(OG) are 113° and 108°, respectively. This indicates that a specific H-bond is formed between Ser47(OG) (donor) and Cys46(O) (acceptor) in correspondence with the free energy profile minimum of the **red** Fd7119 form.

In Figure 5a, all the free energy curves of the oxidized form show strong minima around $\phi_{47} = -100°$, the "CO in" conformation. Specifically, simulation FdO$^{ni}_{ss}$ has a minimum at $\sim -110°$, whereas for FdO$^{i}_{ss}$ and FdO$^{ni}_{hs}$ the minima are at $\phi_{47} \approx -85°$ and $\phi_{47} \approx -105°$, respectively. It is interesting to point out that weak minima with activation barriers of only 2−3 k_BT are also found for the conformation "CO out". Indeed, as for the simulations in the reduced state, a hydrogen bond between Ser47(OG) (donor) and Cys46(O) is always detected for the "CO out" state.

In contrast with results from the reduced state, we did not detect any specific interactions playing a role at the absolute minima of the oxidized state. Indeed, in the "CO in" conformation the carbonyl does neither point directly to the [2Fe−2S] cofactor—the shortest being with Fe2 at about 3.4 Å—nor to any of the cysteines. Finally, a barrier is found at $\phi_{47} \approx 30°$ for FdO$^{i}_{ss}$ and FdO$^{ni}_{hs}$ and at $\phi_{47} \approx 54°$ for FdO$^{ni}_{hs}$.

The Cys46 carbonyl group can go from the "CO in" to the "CO out" conformations and vice-versa through two possible pathways: We call *internal* and *external* the pathways corresponding to the large and small barriers of the free energy profiles, respectively (see Figure 5).

To identify the protein atoms most involved in unfavorable interactions with the negatively charged Cys46(O) atom (−0.51 *e*), we have analyzed the umbrella sampling trajectories of systems FdR$^{ni}_{ss}$ and FdO$^{ni}_{ss}$ at the top of their *internal* and *external* barriers. For both trajectories and barriers we have counted the atoms in closest contact with Cys46(O) and computed the quantity F_c, or the collisional fraction. F_c is defined as the fraction of the total run time in which a couple of atoms have a distance less than $r_{min}/2$, with r_{min} is the radius of the corresponding van der Waals potential at minimum. The collisional fraction is near 1 when the two atoms are in close contact. Thus, most unfavorable interactions affecting the "CO in"/"CO out" transition will be with negatively charged atoms with high F_c.

In Table 3 we list the atoms and their charges with a high F_c. For system FdR$^{ni}_{ss}$, negatively charged Thr48(N), Leu77-(CD2), and S2 of the [2Fe−2S] cluster, have the highest collisional fraction for the *internal* barrier. For the same barrier, electrostatically attractive interactions also exists with Ser47-(HA) and Ser47(C), the highest in F_c. In contrast, the amide hydrogen Ser47(HN), which rotates at the same time as the carbonyl, experiences very few collisions in both pathways (data not shown). Thus, the free energy barrier of the *internal* and *external* pathways is dominated by repulsive interactions involving the carbonyl, not the amide group.

Results obtained for the *external* free energy barrier in Table 3 show that Ala45(O) and Phe65(CG2) repulsively interact with the Cys46 carbonyl.

For the FdO$^{ni}_{ss}$ system, at the top of the *internal* barrier, the most important repulsive interactions for Cys46(O) are with Ser47(OG) and Thr48(N), whereas only interactions with Ser47(OG) are most unfavorable for the *external* barrier.

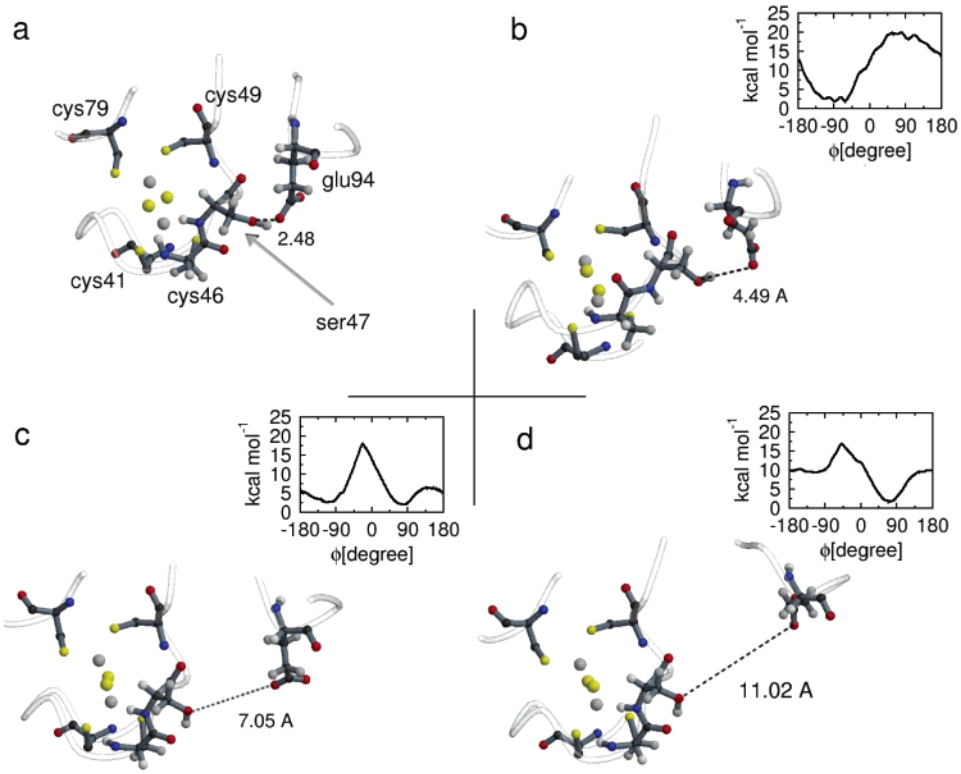

Figure 6. Position of Glu94 with respect to the Ser47 residue shown with the corresponding free energy profiles for the ϕ_{47} torsion angle. Ball-and-sticks are used for Ser47, Glu94 and the four cysteines coordinated to the [2Fe−2S] cluster. Only the trace of the backbone is shown for the remaining residues. Four structures are displayed: In panel **a**, the X-ray structure of ref 12; in panel **b**, the simulated crystal molecul B; in panel **c**, the simulated crystal molecul E; in panel **d**, the simulated crystal molecule A. In each panel, a dashed line joins Ser47(OG) and Glu94(OE) and the distance between these two atoms is reported.

Table 3. Collisional Fractions, or F_c, for Atom Cys46(O)

FdR^{ni}_{ss} atom Cys46(O)							
$\phi_{bias} = -50.0°$				$\phi_{bias} = 170.0°$			
$K_{bias} = 20.0$ kcal mol^{-1}				$K_{bias} = 15.0$ kcal mol^{-1}			
atom	residue	F_c	Q	atom	resisude	F_c	Q
HA	Ser47	0.55	0.09	C	Ala45	0.13	0.51
C	Ser47	0.74	0.51	O	Ala45	0.35	−0.51
N	Thr48	0.21	−0.47	HA	Cys46	0.15	0.09
CD2	Leu77	0.14	−0.27	CA	Ser47	0.75	0.07
S2	[2Fe−2S]	0.2	−0.84	HB2	Ser47	0.91	0.09
				HB2	Phe65	0.1	0.09
				CD2	Phe65	0.2	−0.11
FdO^{ni}_{ss} atom Cys46(O)							
$\phi_{bias} = 30.0°$				$\phi_{bias} = 125.0°$			
$K_{bias} = 20.0$ kcal mol^{-1}				$K_{bias} = 25.0$ kcal mol^{-1}			
atom	residue	F_c	Q	atom	resisude	F_c	Q
CB	Cys46	0.63	0.03	HA	Cys46	0.49	0.09
HB2	Cys46	0.56	0.01	CA	Ser47	0.34	0.09
CA	Ser47	0.64	0.07	HB1	Ser47	0.44	0.09
CB	Ser47	0.14	0.05	OG	Ser47	0.90	−0.66
OG	Ser47	0.24	−0.66				
C	Ser47	0.96	0.51				
N	Thr48	0.60	−0.47				

Only atoms which have $F_c \geq 0.1$ and are not first or second topological neighbors of Cys46(O) are listed. ϕ_{47} and K_{bias} are the parameters used in the biasing potential. Q's are the charges of the atom in the CHARMM27 force field expressed in e. On the left and right-hand sides we list F_c for *internal* and *external* pathways. On the top are results for run FdR^{ni}_{ss} and on the bottom for run FdO^{ni}_{ss}.

According to the free energy profiles shown in Figure 5, the conformational transition between the "CO out" and "CO in" states will most likely occur through the *external* pathway for both **red** and the **oxi** Fd7119 forms. However, only for the **red** form the Cys46(O) atom has a large collisional fraction with atoms belonging to residue Phe65 at the top of the *external* barrier (Table 3).

2. Role of Glu94 on the Free Energy Profiles. As discussed in section 3.1, the H-bond between Glu94(OE2) and Ser47-(OG) found in the crystal is not conserved both in hydrated structures of parsley ferredoxin and in the ferredoxin/FNR complex. Glu94 is located within a group of 3 consecutive negatively charged residues (94−96) occurring near the C-terminus of the protein and interacting electrostatically with the active site, the [2Fe−2S] cluster. In our simulation of hydrated Fd7119, we were not surprised to find residues 94−96 strongly solvated by water to the extent that the distance between their side-chains with the [2Fe−2S] cluster and its neighboring residues is increased. This might well be an artifact of the force field which not including electronic polarization is likely to overestimate water solvation.[33] Another explanation might be an improper screening of the interaction due to the noncomplete equilibration of the positive counterions of the simulation.

To investigate the effect of this interaction on the free energy profile of the "CO in" to "CO out" transition, we have carried out additional simulations of reduced Fd7119 in its crystal environment. Only in this charged state we expect an interesting dependence on the distance between Glu94 and the [2Fe−2S] cluster. Indeed, given the structure of the free energy profile of the oxidized state, the decrease of this distance could only increase the relative stability of the "CO in" conformation.

In this series of simulations, after equilibration (see Section IIA) the distances between Glu94(OE2) and Ser47(OG) in the

8 molecules of the simulation box were computed. As shown in Table 2, a broad spread in these distances was obtained. We notice that the experimental H-bond between Glu94 and Ser47 are not well reproduced. In addition to the previously mentioned force field limitations, this could also be due to inadequacies in the simulated crystallographic environment which included no ions.

Molecules B, E, and A, with Glu94(OE2)-Ser47(OG) distances of 4.49, 7.05, and 11.02 Å, respectively, were chosen to undergo additional free energy calculations. Their ϕ_{47} free energy profiles are reported in Figure 6 along with a pictorial representation of the molecule conformations in their "CO in", molecule B, and "CO out", molecules E and A, states.

We first notice that in Figure 6 the free energy of the Cys46 carbonyl oxygen conformation is strongly dependent on distance between the negatively charged C-terminus residues (in particular Glu94) and the [2Fe−2S] cluster region. Indeed, when the Glu94(OE2)−Ser47(OG) distance is 11.02 Å (panel d), the "CO out" conformation becomes favored and the free energy profile is similar to those computed for the hydrated reduced Fd. Instead, for the shortest distance, 4.49 Å in panel b, the "CO in" is more stable and the free energy curve on the right-hand side of the panel is very much like the one computed for oxidized Fd7119 and presents both a minimum at $\phi_{47} \approx -90°$, and a more pronounced barrier placed at ∼80°.

Interestingly, the profile computed for the intermediate distance of 7.0 Å in panel c presents two minima, at less than a k_BT from each other, corresponding to the "CO in" and the "CO out" conformations. The largest activation is now at $\phi_{47} \approx -24°$ in an intermediate position between the maxima found for the oxidized and reduced Fd7119 simulations. An activation barrier of ∼4.4 kcal mol^{-1} is found for the *external* transition pathway between "CO in" and "CO out".

Thus, the "CO in" and the "CO out" relative stability obtained in our simulation depends on the distance between Glu94 and the region near the [2Fe−2S] cluster. Hence, Glu94 might be thought as a trigger for the transition between "CO in" and "CO out" states in **red** Fd7119.

A closer inspection of the three conformations in panels b, c, and d of Figure 6 reveals that at large Glu94(OE2)−Ser47-(OG) distances the "CO out" conformations present a hydrogen bond between Ser47(OG) and Cys46(O) which disappears in their "CO in" conformations. The origin of this behavior is the hydrogen Ser47(HG1) which is able to interchange its position between favorable interactions with the carboxylate of residue Glu94, "CO in" state, and the H-bond with Cys46(O), "CO out" state. For molecule B, shown in panel b in its "CO in" conformation, the hydrogen bond Ser47(OG)−Cys46(O) does not exist, the Ser47(HG1) pointing toward the Glu94 carboxyl terminal groups.

IV. Conclusions

This paper has reported on the calculation of the free energy profile of the ϕ_{47} backbone angle which control the "CO in" to "CO out" transition in the reduced and oxidized Ferredoxin from Cyanobacterium *Anabaena* PCC7119. Calculations were carried out for Fd7119 in both solution and its crystal environment. The computed free energy curves show a great consistency with each other, despite the different conformational states of the C-terminus region spanned by the different trajectories considered here. These profiles demonstrate that, as in the crystal, in solution the carbonyl oxygen Ser47 can be found in two states: The "CO in" state, stable for **oxi** Fd7119, and the "CO out" state, stable for **red** Fd7119.

Although our molecular dynamic investigation uses a state of the art force field, the electrostatic interactions for a highly charged system such as ferredoxin are likely to be overestimated by an electrostatic model such as ours which lacks contributions from electronic polarization. Indeed, previous works[36,37] have shown that electronic polarization has significant effects on the screening of the electrostatic interactions in redox states. Thus, the repulsion of Ser47 and the [2Fe−2S] cofactor with Glu94 and the other negatively charged C-terminus are not sufficiently screened by our fixed charge model. As a likely consequence, in all our equilibrated structures Glu94 is always farther away from Ser47 than experimentally, in the crystal and in solution.

The free energy profiles obtained in this study are relevant to electron transfers in the PSI/Fd7119 and Fd7119/FNR complexes. In the former, the transfer occurs between PSI and the oxidized form of ferredoxin. According to our results summarized in Figure 5, the "CO in" conformation being the most stable for the **oxi** form (see panel a) will evolve rapidly to the "CO out" state after Fd7119 reduction, panel b, with activation energies of not more than 1 k_BT at 300 K. We assume here that PSI → Fd7119 electron transfer is unaffected by the "CO in" and "CO out" states of ferredoxin. This is unlikely. Indeed, from our calculations the driving force for the electron transfer from PSI to ferredoxin in its "CO in" state is positive and estimated at 6 kcal mol^{-1}.[41] This is a strong indication of a highly activated electron transfer. An activated process is also predicted if the "CO out" conformation *only* can sustain electron transfer. In this last case, our free energy profiles predict an activation energy to go from "CO in" (stable for the **oxi** state) to "CO out" of 11−12 kcal mol^{-1}.

For the Fd7119/FNR complex, our calculations indicate that the most stable state of **red** ferredoxin is the "CO out" state, Figure 5, panel b. When an electron is transferred from Fd7119 to FNR, the "CO out" state ($\phi_{47} \approx 75°$) for **oxi** Fd7119 is metastable, see panel a, and will quickly evolve to the "CO in" state of the **oxi** form with activation energy of at most 3 k_BT.

So far, we have discussed the interplay between electron transfer and conformational changes in Fd7119 based on our results for hydrated ferredoxin. The picture we have depicted can change dramatically if the conformation of ferredoxin is different in the PSI/Fd7119 and Fd7119/FNR complexes than in solution. Indeed, our computations of the ϕ_{47} free energy profile for three different **red** Fd7119 molecules in the reduced crystal environment show that the relative stability of the "CO in" state with "CO out" depends crucially on the distance between the Ser47 and the Glu94 residues. For short distances, the "CO in" state is favored in the **red** form, whereas for large distances the "CO out" state becomes increasingly favored. These findings and the mobility of the C-terminus groups, as seen in our simulations, could change dramatically the free

(41) This value was obtained as follows: First, the driving force for the reaction to reduced ferredoxin in its "CO out" state can be estimated at −3 kcal mol^{-1}, as the midpoint potential of ferredoxin and F_AF_B for PSI from spinach are ≃−9.45 kcal mol^{-1} [38] and ≃−12.45 kcal mol^{-1},[39] respectively. Second, from Figure 5, about +9 kcal mol^{-1} are necessary to go from "CO out" to "CO in" in the reduced ferredoxin. The sum of these two energies is our estimate of the electron transfer from PSI to the "CO in" state of ferredoxin.

energy profile for ϕ_{47} in the complex ferredoxin/PSI with respect to that observed in solution. Hence, conformational changes in Fd7119 when bound to PSI or FNR can have crucial effects on the kinetics of the electron transfer.

Essential to the relative stability of the "CO in" and "CO out" states is the hydrogen bond between between Ser47(OG) and Cys46(O) which locks in the "CO out" state. These findings can provide an interpretation of site-directed mutagenesis experiments by Hurley et al.[38] which demonstrated that only the Ser47Thr Fd7119 mutant had electron transfer activity (50 % of the wild type) in the Fd/FNR complex. Indeed, only residues serine and threonine can switch between a specific hydrogen bond with Cys46(O) and an interaction with Glu94.

To conclude, our simulations have shown a relevant role for Phe65 in the "CO in" to "CO out" transition of the **red** form of Fd7119. Indeed, we find that Phe65 has a large probability of colliding with the Cys46(O) at the top of the *external* barrier. Thus, our calculation predicts that the electronic shells of the carbonyl Cys46 group and the phenyl ring in Phe65 are in close contact during the conformational transition. This finding is relevant to the electron transfer between the reduced form of Fd7119 and the FAD isoalloxazines of FNR. Indeed, the carbonyl/phenyl ring interaction could facilitate the de-localization of the Fd's electron toward the Π orbitals of Phe65 aromatic ring which is found to be crucial to the Fd7119/FNR electron transfer.[9,15]

Acknowledgment. F.P. and M.M. would like to thank Andrea Giansanti for continuous encouragement all along the development of this study.

JA0370286